Visual and Hydrodynamic Feedback Control of a Robotic Fish for Inline Swimming [⋆]

Wei-Kuo Yen [*] **Kruti Bhingradiya** [**] **Tony Regli** [**]
Derek A. Paley [***]

[*] *MATRIX Lab, University of Maryland, California, MD 20619 USA (e-mail:wyen@umd.edu).*
[**] *Department of Aerospace Engineering, University of Maryland, College Park, MD 20742 USA (e-mail: krutib26@umd.edu, tregli@terpmail.umd.edu)*
[***] *Department of Aerospace Engineering and Institute for Systems Research, University of Maryland, College Park, MD 20742 USA (e-mail: dpaley@umd.edu)*

Abstract: This paper develops a method to control the downstream position of the sensor-equipped follower in a pair of two robotic fish swimming in an inline configuration. To swim against the incoming flow, the follower estimates the relative flow velocity using a Bayesian filter with pressure measurements and sets it as the reference to control its flapping amplitude. To maintain its downstream position relative to the leader, the follower extracts the oscillation frequency, phase, and separation distance of the leader from onboard camera images. Water tunnel experiments confirm the feasibility of using hydrodynamic and visual measurements for swimming speed and downstream position control.

Keywords: Autonomous underwater vehicles, perception and sensing, estimation and filtering, output feedback control, bioinspired robotics

1. INTRODUCTION

The schooling behavior of fish inspires the design of formation control of autonomous underwater vehicles (Paley et al., 2007) and has been applied to adaptive ocean sampling (Leonard et al., 2007). One of the benefits of schooling for fish is the increase of their propulsive efficiency (Weihs, 1973; Ashraf et al., 2017). While schooling, fish may maintain a diamond or a phalanx formation and keep their tail motions in or out of phase with their neighbors' motions, so that they can utilize the shed vortices generated by their neighbors. To understand how the hydrodynamic mechanism of schooling works, and the roles of flapping kinematics and flow interactions, experiments of flapping foils with inline configuration have been performed (Newbolt et al., 2019). Their results show that the temporal flapping phase between two foils and the spatial phase shift between their trajectories are keys to achieving group cohesion. The follower can obtain hydrodynamic benefits inside the thrust wake generated by the leader as it swims with the local lateral flow instead of against it (Zhu et al., 2014). This phenomenon, also called vortex phase matching, has been applied to a pair of fish robots to obtain hydrodynamic benefits (Li et al., 2020).

To maintain group structure while schooling, each fish receives the relative states of its neighbors and flowfield information via visual and lateral line systems (Pitcher

et al., 1976). Equipment that assists with positioning and tracking for fish-inspired robots includes cameras and hydrodynamic sensors. Applications of visual sensing on fish robots include optimization of the swimming gait (Wang et al., 2017), obstacle detection and avoidance (Kelasidi et al., 2019), and three-dimensional formation control (Berlinger et al., 2021). For hydrodynamic sensing, related research includes station holding in a steady or unsteady flow (Salumäe and Kruusmaa, 2013; Krieg et al., 2019), relative position estimation of a nearby robot (Yen et al., 2020), wall following (Yen et al., 2018), Kármán gaiting (Free and Paley, 2018), and formation control of a group of robotic fish (Wolek and Paley, 2023). Although previous research has demonstrated the applications of visual and hydrodynamic sensing in underwater robots, few studies have applied both techniques to control the formation of fish robots.

This work describes feedback control of the follower fish in a pair of two robotic fish swimming in an inline configuration in a uniform flow using visual and hydrodynamic measurements. The follower is instrumented with a camera and a pressure sensor array. To estimate the relative flow velocity, a pressure difference model based on the two-dimensional (2D) potential flow is developed as the measurement model of a grid-based Bayesian filter (Zhang et al., 2015). After incorporating the pressure measurements from the pressure sensors, the velocity estimate is converted to the flapping amplitude of the follower via inverse kinematics so that it can swim against the in-

coming flow. The oscillation frequency, phase, and relative position of the leader are converted from the changes in the intensity and size of the leader body in time-series images captured by its onboard camera using contour detection, a pin-hole camera model, and the discrete Fourier transform (Bradski and Kaehler, 2008). To reduce the self-motion effect on visual sensing, the follower swims intermittently and performs visual sensing while coasting. The obtained information is input to a central pattern generator (Seo et al., 2010) to generate the reference flapping behavior for the follower to maintain its downstream position and flapping phase relative to the leader. To date, two experiments have been conducted to validate the method: (1) the follower controls its flapping amplitude to swim against the flow using hydrodynamic feedback; and (2) the follower maintains its downstream position relative to the leader using visual feedback.

The contributions of this paper are (1) an image-based method to obtain the relative distance, oscillation frequency, and phase of a leader fish using an onboard camera and (2) a perception-based feedback controller using visual and hydrodynamic measurements to regulate the downstream separation of the follower fish in an inline swimming configuration. These contributions help to develop fish robots that are capable of using sensing feedback to maintain their group structure.

This work is organized as follows. Section 2 presents the flow field model of a single robot and Bayesian estimation for flow sensing. Section 3 describes the image processing procedures for measuring the separation distance, oscillation frequency, and relative phase between two fish robots. Section 4 presents the dynamic modeling of the robot, the design of the controllers using visual and hydrodynamic feedback, and the experimental results. Section 5 summarizes the results and ongoing work.

2. FLOW ESTIMATION BY PRESSURE SENSING

This section describes the 2D potential flow model for a robotic fish swimming in a uniform flow and flow estimation using grid-based Bayesian filtering. First, the robot is approximated as a Joukowski foil transformed from a circle through conformal mapping. Then, the pressure model of this robot is derived from its complex potential model using Bernoulli's equation. Finally, this pressure model is set as the measurement model of a grid-based Bayesian filter to estimate the relative flow velocity and angle of attack using pressure difference measurements on the surface of the robot.

2.1 Conformal Mapping and Complex Potential Functions

To obtain the state of the flow field around the follower, a hydrodynamic model based on two-dimensional potential flow theory (Panton, 2005) is used. The definitions of the coordinates are shown in Fig.1. The xy frame is located at the center of rotation of the robot. This robot is described as a Joukowski foil in the physical z-plane mapped from a circle centered at ζ_0 with radius R in the complex ζ-plane through the following Joukowski transform

$$z = \zeta + \frac{a^2}{\zeta} - z_O^0, \tag{1}$$

where $a = l/4$ is one-quarter chord length of the foil and $R = |a - \zeta_0|$; z_O^0 is the origin of the xy frame described in the z_0-plane. Suppose the foil rotates with velocity Ω about the pivot point O in a flow field with uniform flow speed U_f, the complex potential of the foil (Zhang et al., 2015) without considering shed vortices is

$$F(\zeta) = U(\zeta - \zeta_0)e^{-i\alpha} + U\frac{R^2}{\zeta - \zeta_0}e^{i\alpha} + \Omega F_\Omega \\ + i\frac{\Gamma_0}{2\pi}\ln\left(\frac{\zeta - \zeta_0}{R}\right) \tag{2}$$

$$F_\Omega = -\frac{i}{2}\left(R^2 + 2\zeta_0\frac{R^2}{\zeta - \zeta_0} + |\zeta_0|^2 \\ + 2a^2\left(\frac{R^2}{\zeta^2 - \zeta\zeta_0} + \frac{\overline{\zeta_0}}{\zeta}\right) + 2z_O^0\frac{R^2}{\zeta} + 2\overline{z_O^0}\left(\zeta_0 + \frac{a^2}{\zeta}\right) \\ + z_O^0\overline{z_O^0} + \frac{a^4(\zeta - 2\zeta_0)}{\zeta(R^2 - |\zeta_0|^2)}\right), \tag{3}$$

where $\Gamma_0 = 4\pi R U \sin\alpha$ is the vortex circulation generated on the foil.

The robot is equipped with N_p pressure sensors located at the positions $z_{p1}, ..., z_{pi}$. For steady, inviscid, incompressible, and irrotational fluid, the pressure difference between two sensors located at positions z_i and z_j is calculated using Bernoulli's equation (Panton, 2005):

$$\Delta p_{ij} = \frac{\rho}{2}\left(\left|W(z_{p_j})\right|^2 - |W(z_{p_i})|^2\right), \tag{4}$$

where ρ is the density of water and $W(z_{p_i}) = \mathrm{d}F/\mathrm{d}z$ is the complex velocity at point z_{p_i} in the z-plane. These measurements are used for flow estimation.
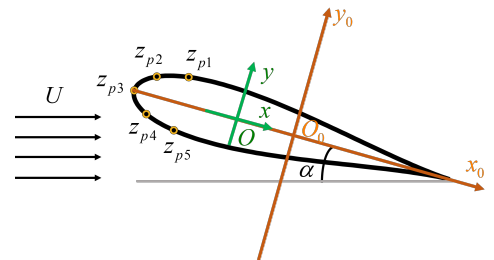

Fig. 1. Coordinate systems of the fish robot including the locations $z_{p1}, ..., z_{p5}$ of the pressure sensors.

2.2 Flow Estimation using Bayesian Filter

A recursive, grid-based Bayesian filter (Arulampalam et al., 2002) estimates the relative flow speed U and angle of attack of the follower α from the flow measurements. For the grid-based method, the state space is assumed to be discrete and consists of a finite number of discrete states $\mathbf{x} = [U, \alpha]^T$. At each time step, flow measurements are assimilated recursively to infer the most likely state vector $\hat{\mathbf{x}}$ by calculating its probability. The N_p pairs of pressure differences between sensors are set as the flow

measurements $\mathbf{y} = [\Delta p_{12}, ..., \Delta p_{N_p-1 N_p}]^T$. Then, the instantaneous measurement equation is

$$\mathbf{y} = H(\mathbf{x}) + \eta, \qquad (5)$$

where H is the nonlinear function from (4) and η is the zero-mean Gaussian sensor noise with variance σ. For the grid-based Bayesian filter with Gaussian measurement noise, the likelihood function is

$$\pi(\mathbf{y}|\mathbf{x}) = \frac{1}{\sqrt{(2\pi)^2 \det(\mathbf{R}_s)}} \\ \times \exp\left[-\frac{1}{2}(\mathbf{y} - H(\mathbf{x}))^T \mathbf{R}_s^{-1}(\mathbf{y} - H(\mathbf{x}))\right], \qquad (6)$$

where $\mathbf{R}_s$ is the covariance matrix of the measurement. The posterior probability density function (PDF) at time k is obtained by using the Bayesian formula with the likelihood function and the prior PDF:

$$\pi(\mathbf{x}_k|\mathbf{y}_{1:k}) = \kappa \pi(\mathbf{y}_k|\mathbf{x}_k) \pi(\mathbf{x}_k|\mathbf{y}_{1:k-1}), \qquad (7)$$

where κ is the factor normalizing the integration of the total posterior probability to one. After incorporating the new measurement, the posterior becomes the prior for the next time step.

To model the process noise of the system, the PDF is convolved with an n_c-dimensional, zero-mean Gaussian kernel as a numerical approximation of the Fokker-Planck equation with diffusion only (Free and Paley, 2018). This operation has a gradual blurring effect on the PDF. Without any new measurements, the PDF becomes a uniform distribution as time goes to infinity.

3. LEADER ESTIMATION BY VISUAL SENSING

This section describes an image processing method for the follower to obtain the states of the leader including oscillation frequency, phase, and the relative distance. The concept is to convert the pixel size of the leader body and the changes in the image intensity due to its flapping motion to the state information using a pinhole camera model and the discrete-time Fourier transform.

Figure 2 shows the experimental platform and the robots. Both robots are 43 cm in length and are composed of a rigid head and a flexible tail. Each of the robots is connected to a rigid shaft driven by a servo motor. The leader is mounted on the frame of the water tunnel, so it can only perform yaw motion. The follower is attached to a cart with linear frictionless air bearings to generate yaw and surge motions.

3.1 Frequency and Phase of the Leader

To obtain the flapping frequency and phase of the leader from the video sequences, we first use the contour detection function of OpenCV (Bradski and Kaehler, 2008) to detect the body contour of the leader. This function is able to find the edge of the fish body in an image, providing the related
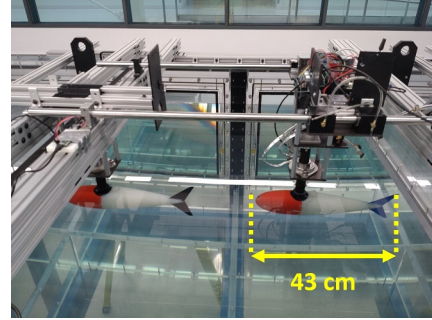

Fig. 2. Experimental platform of two robotic fish with inline configuration. The leader is mounted on the frame of the water tunnel and the follower is attached to a cart with linear air bearings.

position and size in the image frame. To ensure the fish body is picked up by the detector, some image processing procedures are performed as shown in Fig. 3. Since contour detectors usually work best on binary black-and-white images, the original image (Fig. 3(a)) is first converted to a binary image (Fig. 3(b)) with an image threshold, where any pixel brighter(darker) than the threshold gets set to white(black). This binary image is then blurred to reduce the noise from bubbles (Fig. 3(c)) and is cropped to isolate the fish body (Fig. 3(d)).

Because the leader oscillates its body in the horizontal plane periodically, we record the x position of its body contour in the image frame and then extract the oscillation frequency from these time-series signals using the discrete Fourier transform. The discrete Fourier transform returns a list of the frequencies with corresponding amplitudes that make up the oscillation. The frequency with maximum amplitude is then set as the feedback frequency. The phase between the leader and follower oscillations can be found by using cross-correlation, which is used to find the phase that maximizes the correlation.
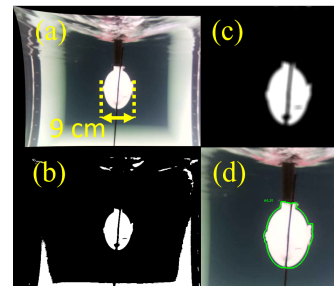

Fig. 3. Edge detection of the leader. (a) Original image captured by the camera on the follower. (b) Original image converted to the binary image. (c) Binary image after blurring and cropping. (d) Processed image with the edge found by the countour detection function.

3.2 Separation Distance between the Leader and Follower

The separation $\hat{D}$ between the leader and follower from the visual measurement can be calculated by using the pinhole camera model based on similar triangles (Bradski and Kaehler, 2008):

$$\hat{D} = \frac{H_l \cdot F_c}{P_l} + D_{cs}, \qquad (8)$$

where F_c is the distance from the pinhole aperture to the image plane in pixels, which can be can be obtained from an object with known distance and height; H_l is the height of the leader body in the physical plane; P_l is the pixel height of the leader body in the image plane; and D_{cs} is the distance between the camera and the shaft of the follower.

4. FEEDBACK CONTROL IMPLEMENTATION AND RESULTS

Experiments conducted in a circulated water tunnel using two robotic fish were carried out to demonstrate the proposed control strategy. First, the experimental setup and the inverse kinematics for the swimming speed of the robot are described. Then, the control system for the follower using visual and hydrodynamic feedback is presented. Finally, the experiments of speed and separation controls using hydrodynamic and visual feedback are demonstrated, respectively.

4.1 Inverse Kinematics for Robotic Fish Swimming Speed

Both robotic fish consist of a rigid head printed with PLA and a flexible tail made up of silicone rubber. The leader and follower are controlled by a microcontroller and a single-board computer, respectively. The leader is mounted on the frame of the water tunnel, and the follower is attached to a cart with linear frictionless air bearings. An ultrasonic distance sensor is equipped on the cart to record the separation distance between the leader and follower. Both leader and follower are actuated by the brushless DC motors with speed controllers. The follower has an endoscope camera with a frame rate of 16 fps inside its head and five pressure sensors whose positions are indicated in Fig. 1.

To determine feed-forward control input, experiments were conducted to determine and verify a dynamic model for the follower robot swimming alone. The follower starts flapping at a predetermined frequency with a varying amplitude until it finds an amplitude to hold its along-stream position to counter the flow speed. Once the flapping response settles, the amplitude for that flow speed and frequency is noted. A set of flapping amplitude data for varying frequencies to counteract varying flow velocities is obtained. When the flow velocity is set to the desired swimming speed, this setup aids in determining the flapping frequencies and amplitudes for that specific swimming speed. The inverse relationship between flapping amplitude and frequency was obtained from the experiments with varying swimming speeds as shown in Fig, 4. To predict the amplitude A for given swimming speed U and frequency f, a multiple linear regression model based on the experimental data and (Zhong et al., 2017) is derived:

$$A(U, f) = 5.48 + 0.49U - 6.79f. \qquad (9)$$

Frequency, Phase, and Separation Controls To maintain the along-stream position and motion of the follower rel-
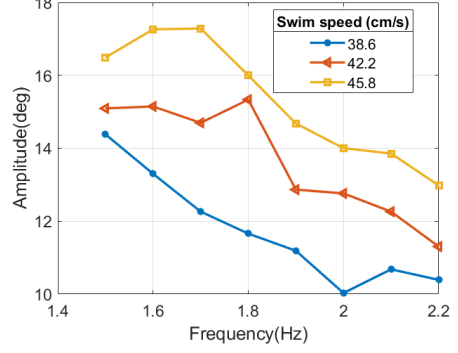

Fig. 4. Experimentally determined amplitude vs. frequency for varying swimming speeds.

ative to the leader, the control system shown in Fig. 5 includes separation control and phase-following control. For separation control, the follower controls its swimming speed by adjusting its frequency and amplitude of oscillation using visual and hydrodynamic feedback. The control amplitude A_0 for the robot to achieve a specific swimming speed is obtained using (9):

$$A_0 = A(\hat{U}, f_F), \qquad (10)$$

where $\hat{U}$ is the relative flow speed estimated from the grid-based filter with pressure measurements as described in (7) in section 2; and f_F is the oscillation frequency of the follower which is set as the oscillation frequency of the leader $\hat{f}_L$ obtained from the camera. To compensate for the unmodeled dynamics, a proportional feedback controller is set as

$$\Delta A = K_P \left(D_t - \hat{D} \right), \qquad (11)$$

where ΔA is the control amplitude variation; $K_P < 0$ is the proportional control gain; D_t is the separation command. Then, the angle command input to the follower is the sum of (10) and (11), i.e.,

$$\rho_F = A_0 + \Delta A. \qquad (12)$$

Since leader and follower oscillate their bodies periodically, their reference angular positions r_L and r_F are generated from Hopf oscillators (Seo et al., 2010). The benefit of using the Hopf oscillator includes continuous and smooth transitions among different gaits due to its limit cycle behavior. To control the phase of the follower relative to the leader, the oscillators can be connected by a directional diffusive coupling and the follower receives a control input designed based on the states of the leader.

To enable the robots follow the reference trajectories to oscillate their bodies, PI feedback controllers are chosen as follows:

$$I_i = K_{Pi}\Delta\theta_i + K_{Ii} \int \Delta\theta_i \, dt, \qquad i = L, F \qquad (13)$$

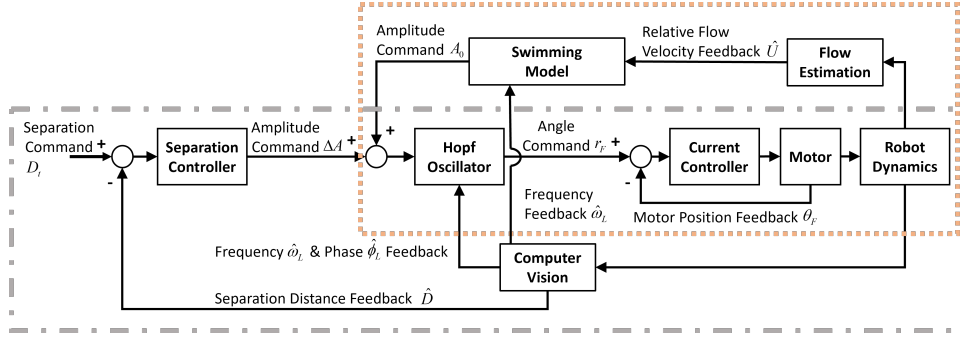where I_i is the current command input to the motor and $\Delta\theta_i = r_i - \theta_i$.

Fig. 5. Block diagram of the control system. The speed control using hydrodynamic feedback (orange) and separation control (grey) using visual feedback are inside the dotted and dash-dotted boxes, respectively.

4.2 Speed Control using Hydrodynamic Feedback

Here we present the experimental results of controlling the oscillation amplitude of the robot to swim against the incoming flow using hydrodynamic feedback. The block diagram of the control system is shown inside the orange dashed square in Fig. 5. Figure 6 (a) shows the position of the robot recorded by the ultrasonic distance sensor and Figs. 6 (b) and (c) show the estimation results of the relative flow speed and angle of attack. The robot started oscillating its body at a frequency of 2 Hz at $t = 30$ s and the feedback control started at $t = 40$ s. The water tunnel speed started at 0.34 m/s at $t = 30$ s, raised to 0.44 m/s at $t = 60$ s, dropped to 0.27 m/s at $t = 90$ s, and then stopped at $t = 140$ s. The processing rate of estimation and control was 10 Hz, and the pressure signals were filtered with a moving-average window with a window size of 0.2 s. There is a delay in both estimated signals due to the usage of a quasi-steady model and the delay of filtering. The relative flow speed was estimated using the grid-based filter described in Section 2 and was mapped by (10) to derive the required oscillation amplitude for the robot. Then the desired amplitude was set to the controllers in (12–13). The underprediction of flow velocity during $t = 60 - 90$ s caused the robot to be pushed back by the flow.

4.3 Separation Control using Visual Feedback

Here we present the experimental results of controlling the follower to maintain its separation distance relative to the leader with inline configuration using visual feedback. The block diagram of the control system is shown inside the grey dash-dotted square in 5, and the control formulas are shown in (11–13). The separation distance between two robots is obtained by the camera on the follower using 8 as described in Section 3. We set the follower to swim intermittently, similar to a fish performing burst-and-cost swimming for energy economy (Fish et al., 1991). The follower only performs visual sensing during the coast phase (for 1 s) such that the self-motion effect is smaller. After another 1 s for transition, these visual measurements were averaged and fed back during the burst phase (for 4 s) to control the oscillating amplitude of the follower. Figure 7 shows the separation measurements from the ultrasonic distance sensor (blue line) and the onboard camera of the follower (orange dots). The black dashed line is the target separation distance. There were some moments (within
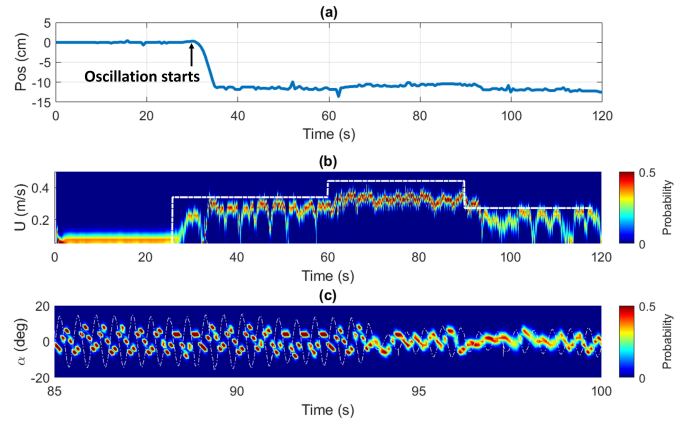

Fig. 6. Experimental results of relative flow feedback control. (a) Along-stream position of the robot recorded by the ultrasonic distance sensor. (b) Probability density of the relative flow velocity from the Bayesian estimator with the tunnel flow velocity (white dash-dotted line). (c) Probability density of the angle of attack with the heading of the robot (white dash-dotted line).

grey dashed frames) during the coast phase when the follower could not detect the whole contour of the leader and made an inaccurate measurement. The follower came too close to the leader during the burst phase because its feedback was based on measurements taken in the previous coast phase. This issue can be mitigated by relocating the camera closer to the nose of the head, using a smaller control gain and shorter burst phase duration, or using hydrodynamic feedback for close-distance control. Overall, the follower tracks to the target distance.

5. CONCLUSION

This work develops a method that uses visual and hydrodynamic feedback to control the relative position of the follower to the leader of two robotic fish swimming in an inline configuration. The follower equipped with a pressure sensor array is capable of sensing the relative flow speed and adjusting its flapping amplitude to swim against the flow. The onboard camera provides the relative position of the leader that can be used as feedback to control the separation distance between two robots. Experimental results show the feasibility of these two types of control. Ongoing work focuses on incorporating visual and hydrodynamic
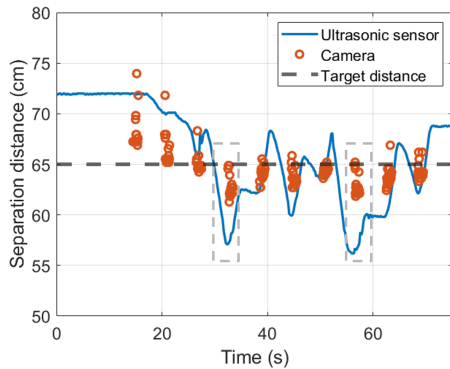
Fig. 7. Separation control between two robots as the follower swims intermittently. The orange dots are the separation measurements from the onboard camera of the follower during the coast phase, and they were fed back during the burst phase for the control. The black dashed and blue lines are the target distance and measurement from the ultrasonic distance sensor, respectively. The inaccurate measurements occurred (within the grey dashed frames) as the follower came too close to the leader.

feedback to control the follower to achieve phase locking with the leader while maintaining its downstream position.

ACKNOWLEDGEMENTS

REFERENCES

Arulampalam, M.S., Maskell, S., Gordon, N., and Clapp, T. (2002). A tutorial on particle filters for online nonlinear/non-Gaussian Bayesian tracking. *IEEE Transactions on Signal Processing*, 50(2), 174–188.

Ashraf, I., Bradshaw, H., Ha, T.T., Halloy, J., Godoy-Diana, R., and Thiria, B. (2017). Simple phalanx pattern leads to energy saving in cohesive fish schooling. *Proceedings of the National Academy of Sciences*, 114(36), 9599–9604.

Berlinger, F., Gauci, M., and Nagpal, R. (2021). Implicit coordination for 3d underwater collective behaviors in a fish-inspired robot swarm. *Science Robotics*, 6(50), eabd8668.

Bradski, G. and Kaehler, A. (2008). *Learning OpenCV: Computer vision with the OpenCV library.* " O'Reilly Media, Inc.".

Fish, F.E., Fegely, J.F., and Xanthopoulos, C.J. (1991). Burst-and-coast swimming in schooling fish (notemigonus crysoleucas) with implications for energy economy. *Comparative Biochemistry and Physiology Part A: Physiology*, 100(3), 633–637.

Free, B.A. and Paley, D.A. (2018). Model-based observer and feedback control design for a rigid joukowski foil in a kármán vortex street. *Bioinspiration & Biomimetics*, 13(3), 035001.

Kelasidi, E., Moe, S., Pettersen, K.Y., Kohl, A.M., Liljebäck, P., and Gravdahl, J.T. (2019). Path following, obstacle detection and obstacle avoidance for thrusted underwater snake robots. *Frontiers in Robotics and AI*, 6, 57.

Krieg, M., Nelson, K., and Mohseni, K. (2019). Distributed sensing for fluid disturbance compensation and motion control of intelligent robots. *Nature Machine Intelligence*, 1(5), 216–224.

Leonard, N.E., Paley, D.A., Lekien, F., Sepulchre, R., Fratantoni, D.M., and Davis, R.E. (2007). Collective motion, sensor networks, and ocean sampling. *Proceedings of the IEEE*, 95(1), 48–74.

Li, L., Nagy, M., Graving, J.M., Bak-Coleman, J., Xie, G., and Couzin, I.D. (2020). Vortex phase matching as a strategy for schooling in robots and in fish. *Nature Communications*, 11(1), 5408.

Newbolt, J.W., Zhang, J., and Ristroph, L. (2019). Flow interactions between uncoordinated flapping swimmers give rise to group cohesion. *Proceedings of the National Academy of Sciences*, 116(7), 2419–2424.

Paley, D.A., Leonard, N.E., Sepulchre, R., Grunbaum, D., and Parrish, J.K. (2007). Oscillator models and collective motion. *IEEE Control Systems Magazine*, 27(4), 89–105.

Panton, R.L. (2005). *Incompressible Flow*. John Wiley& Sons.

Pitcher, T.J., Partridge, B.L., and Wardle, C.S. (1976). A blind fish can school. *Science*, 194(4268), 963–965.

Salumäe, T. and Kruusmaa, M. (2013). Flow-relative control of an underwater robot. *Proceedings of the Royal Society A: Mathematical, Physical and Engineering Science*, 469(2153), 1–19.

Seo, K., Chung, S.J., and Slotine, J.J.E. (2010). Cpg-based control of a turtle-like underwater vehicle. *Autonomous Robots*, 28, 247–269.

Wang, W., Gu, D., and Xie, G. (2017). Autonomous optimization of swimming gait in a fish robot with multiple onboard sensors. *IEEE Transactions on Systems, Man, and Cybernetics: Systems*, 49(5), 891–903.

Weihs, D. (1973). Hydromechanics of fish schooling. *Nature*, 241(5387), 290–291.

Wolek, A. and Paley, D.A. (2023). Output feedback formation control of a school of robotic fish with artificial lateral line sensing. In *2023 IEEE/RSJ International Conference on Intelligent Robots and Systems (IROS 2023)*.

Yen, W.K., Huang, C.F., Chang, H.R., and Guo, J. (2020). Localization of a leading robotic fish using a pressure sensor array on its following vehicle. *Bioinspiration & Biomimetics*, 16(1), 016007.

Yen, W.K., Martinez, S.D., and Guo, J. (2018). Controlling a robotic fish to swim along a wall using hydrodynamic pressure feedback. *IEEE Journal of Oceanic Engineering*, 43(2), 369–380.

Zhang, F., Lagor, F.D., Yeo, D., Washington, P., and Paley, D.A. (2015). Distributed flow sensing for closed-loop speed control of a flexible fish robot. *Bioinspiration & Biomimetics*, 10(6), 065001.

Zhong, Y., Li, Z., and Du, R. (2017). A novel robot fish with wire-driven active body and compliant tail. *IEEE/ASME Transactions on Mechatronics*, 22(4), 1633–1643.

Zhu, X., He, G., and Zhang, X. (2014). Flow-mediated interactions between two self-propelled flapping filaments in tandem configuration. *Physical Review Letters*, 113(23), 238105.